

## MR Line-scan Diffusion Imaging of the Spinal Cord in Children

Richard L. Robertson, Stephan E. Maier, Robert V. Mulkern, Sridhar Vajapayam, Caroline D. Robson, and Patrick D. Barnes

**Summary:** Diffusion imaging has been widely used in the brain, but its application in the spinal cord has been limited. Using line-scan diffusion imaging (LSDI), a technique that is less sensitive to magnetic susceptibility and motion artifacts than are other diffusion techniques, we have successfully imaged the spinal cord in children. The apparent diffusion coefficient and relative diffusion anisotropy of the normal spinal cord were measured. LSDI was compared with echo-planar diffusion imaging of the spine in three patients.

Diffusion imaging of the brain is now a well-established technique (1–3). Diffusion imaging of the spinal cord, however, has proved more challenging. Echo-planar diffusion imaging (EPDI) has had limited application in the spine because of its relatively low spatial resolution and artifacts due to magnetic susceptibility effects. Pulsed-gradient spin-echo diffusion imaging is sensitive to motion and requires approximately 15 minutes to image a single diffusion axis (4). By contrast, line-scan diffusion imaging (LSDI) is a conventional spin-echo-based technique that is relatively insensitive to magnetic susceptibility effects and to bulk motion and can provide imaging of six diffusion axes in as little as 25 seconds per section (5, 6). These properties make LSDI well suited to spinal cord imaging in children.

### Description of Technique

LSDI was performed in 12 children, ages 2 months to 18 years, and in one adult volunteer. Three children were also evaluated with EPDI. LSDI of the cervical spine was performed in six patients, of the thoracic spine in four patients, of the lumbar spine in one patient, and of the entire spine in one patient. The examinations were performed on either a Sig-

na high-speed or LX echo-speed (General Electric Medical Systems, Milwaukee, WI) 1.5-T imaging system.

### LSDI Parameters

The LSDI technique has been previously described (5). Images of the patients were obtained using a quadrature head coil, a phased-array spine coil (General Electric Medical Systems), or a volume neck surface coil (Intermagnetic General Corporation, Medical Advances Inc., Milwaukee, WI). LSDI was performed in either the sagittal or axial plane by using an effective 2014/95/1 (TR/TE/excitations) or 2014/103/1, a  $20 \times 15$ -cm field of view, a 4-mm section thickness,  $128 \times 96$  columns, and a  $b$  of 5 and  $750 \text{ s/mm}^2$ , with the maximum  $b$  value applied in three or six directions. The total imaging time using these parameters was 43 or 86 seconds, respectively, per anatomic location. The appendix provides the exact three and six diffusion sensitization configurations used, the precise relationships between the diffusion coefficients measured along each direction and the diffusion tensor elements, and how the trace apparent diffusion coefficient (ADC) is obtained with either approach. Cardiac gating, respiratory compensation, and first-order gradient moment nulling (flow compensation) were not used.

### Field-of-view Comparison

In the thoracic spine of an adult volunteer, LSDI was performed using a  $30 \times 15$ -cm field of view (2912/76/1,  $128 \times 64$  columns, 4-mm section thickness,  $b$  maximum =  $750 \text{ s/mm}^2$ , six directions, 50 s per location) and using a  $30 \times 7.5$ -cm field of view (1456/76/1,  $128 \times 32$  columns, 4-mm section thickness,  $b$  maximum =  $750 \text{ s/mm}^2$ , six directions, 25 s per location) (Fig 1).

### EPDI Parameters

In addition to LSDI, EPDI was performed in three patients by using a single-shot technique with parameters of 4999/108/1, a  $24 \times 24$ -cm field of view, a 5-mm section thickness, a  $128 \times 128$  matrix, and a  $b$  of 0 and  $1000 \text{ s/mm}^2$ , applied in three orthogonal directions,  $x$ ,  $y$ , and  $z$ .

### LSDI Postprocessing and Image Analysis

Isotropic high  $b$  factor diffusion images were generated from the three or six diffusion directions sampled. These images were calculated as the cubed or sixth root, respectively, of the product of the signal intensities of the different directions obtained with  $b = 750 \text{ s/mm}^2$  extrapolated to  $1000 \text{ s/mm}^2$ . Trace ADC maps were made using the equation presented by Stejskal and Tanner (7),  $S = S_0 e^{-bADC}$ , where  $b$  is the diffusion weighting factor,  $S$  is the signal intensity of the diffusion trace for  $b =$  maximum, and  $S_0$  is the signal intensity for  $b = 5 \text{ s/mm}^2$ .

ADC measurements for the normal spinal cord and for focal lesions were made from the trace ADC maps by using regions of interest (ROIs) positioned over the spinal cord, taking care to avoid inclusion of cerebrospinal fluid. When a focal spinal

Received September 15, 1999; accepted after revision January 19, 2000.

From the Department of Radiology (R.L.R., R.V.M., S.V., C.D.R., P.D.B.), Children's Hospital Medical Center and Harvard Medical School, and the Department of Radiology (S.E.M.), Brigham and Women's Hospital and Harvard Medical School, Boston, MA.

This investigation was aided by a grant from the Whitaker Foundation.

Address reprint requests to Richard L. Robertson, MD, Department of Radiology, Children's Hospital Medical Center, 300 Longwood Avenue, Boston, MA 02115.



FIG 1. Comparison of LSDI images of the thoracic spine in a healthy adult volunteer shows comparable quality.

A, Half field of view (64 columns). Sagittal LSDI isotropic high  $b$  factor image (2912/76/1,  $128 \times 64$  columns, 4-mm section thickness,  $b = 750$  s/mm<sup>2</sup> extrapolated to 1000 s/mm<sup>2</sup>, six directions) using a  $30 \times 15$ -cm field of view and an imaging time of 50 s per location.

B, Quarter field of view (32 columns). Sagittal LSDI isotropic high  $b$  factor image (1456/76/1,  $128 \times 32$  columns, 4-mm section thickness,  $b = 750$  s/mm<sup>2</sup> extrapolated to 1000 s/mm<sup>2</sup>, six directions) using a  $30 \times 7.5$ -cm field of view and an imaging time of 25 s per location.

cord lesion was present, measurements were made from an ROI within the lesion as well as from an ROI of the "normal" spinal cord (no obvious abnormality on either the conventional MR sequences or the diffusion images).

In addition to calculating the trace ADC, a measure of relative anisotropy (RA), defined as the ratio of the maximum to minimum ADC obtained from separate ADC measurements made along the three to six directions of the diffusion-sensitizing gradients, was generated. In the patients in whom focal abnormalities were shown, the RA of the lesion was also determined.

In the three patients in whom both LSDI and EPDI were performed and in the volunteer in whom a 0.5 field of view was compared with a 0.25 field of view, signal-to-noise ratios (SNRs) for the spinal cord were obtained from an ROI positioned over the spinal cord on the average high  $b$  factor diffusion image and an ROI positioned outside of the anatomic image in both the frequency-encode and phase-encode directions. Because of differences in the techniques, the same parameters were not used for the LSDI and EPDI sequences. Rather, both the LSDI and EPDI acquisitions were obtained using parameters routinely used clinically for diffusion imaging of the brain. The SNR comparisons were not adjusted for field of view, acquisition time, matrix, section thickness, or  $b$  value used. The field of view and section thickness used for the two sequences would tend to favor EPDI SNR over LSDI SNR, whereas the acquisition time and maximum  $b$  value used would favor the SNR measurements for LSDI. The image matrix was effectively the same for both LSDI and EPDI. The diffusion images and trace ADC maps were qualitatively assessed by two neuroradiologists for motion artifacts and mag-

netic susceptibility effects (rated as absent, minimal, or marked).

## Results

Only one of the LSDI examinations was considered nondiagnostic because of patient motion. The remaining studies were considered to be of good quality with minimal or absent motion and magnetic susceptibility artifacts. In the three patients for whom both LSDI and EPDI were performed, the mean SNR of LSDI/EPDI was 2.3 (range, 2.0–3.2). In each of these three patients, the EPDI had either marked geometric distortion or artifacts due to magnetic susceptibility effects (Fig 2).

Results of both the conventional MR imaging and LSDI were normal for eight patients and abnormal for three. ADC and RA measurements for the 10 patients with diagnostic quality images that included normal spinal cord are listed in the Table. The mean trace ADC of the normal spinal cord was  $0.96 \pm 0.05$   $\mu\text{m}^2/\text{s}$  SD (range, 0.91–1.06  $\mu\text{m}^2/\text{s}$ ). The mean RA ratio for the normal spinal cord was  $1.70 \pm 0.42$  SD (range, 1.33–2.5). In the patient with suspected radiation effect, the ADC within the lesion was  $0.67$   $\mu\text{m}^2/\text{s}$  (29% less than that of the uninvolved spinal cord) and the RA within the lesion was reduced by 8%. In the patient with cervicomedullary astrocytoma, the ADC within the tumor was  $1.43$   $\mu\text{m}^2/\text{s}$  (35% greater than that of the adjacent uninvolved spinal cord) and the RA within the lesion was reduced by 19%. In the patient with the epidermoid cyst, the cyst had an ADC of 0.54 without appreciable anisotropy. In the adult volunteer for whom LSDI was performed using a 0.5 field of view and a 0.25 field of view, the difference in SNR between the two acquisitions was less than 5% (Fig 1).

## Discussion

These preliminary results indicate that LSDI of the spine is feasible and provides robust diffusion imaging of the pediatric spinal cord without the need for specialized hardware, cardiac gating, or respiratory compensation. Diagnostic quality images of all parts of the spinal cord were obtained using the three coils tested. In all except one of our patients, there were no significant motion artifacts. Importantly, images of the thoracic spine were not significantly degraded by cardiac pulsation or respiratory motion. Magnetic susceptibility artifacts were minimal. In the three patients in whom EPDI was performed for comparison, LSDI had a greater SNR and qualitatively fewer artifacts than did EPDI.

Our observation of diffusion anisotropy within the normal spinal cord of children concurs with *in vitro* and *in vivo* animal experiments in the rat, pig, cat, and mouse and is similar to the results presented by Clark et al (4), who reported *in vivo* spinal cord diffusion imaging in humans achieved using a nav-

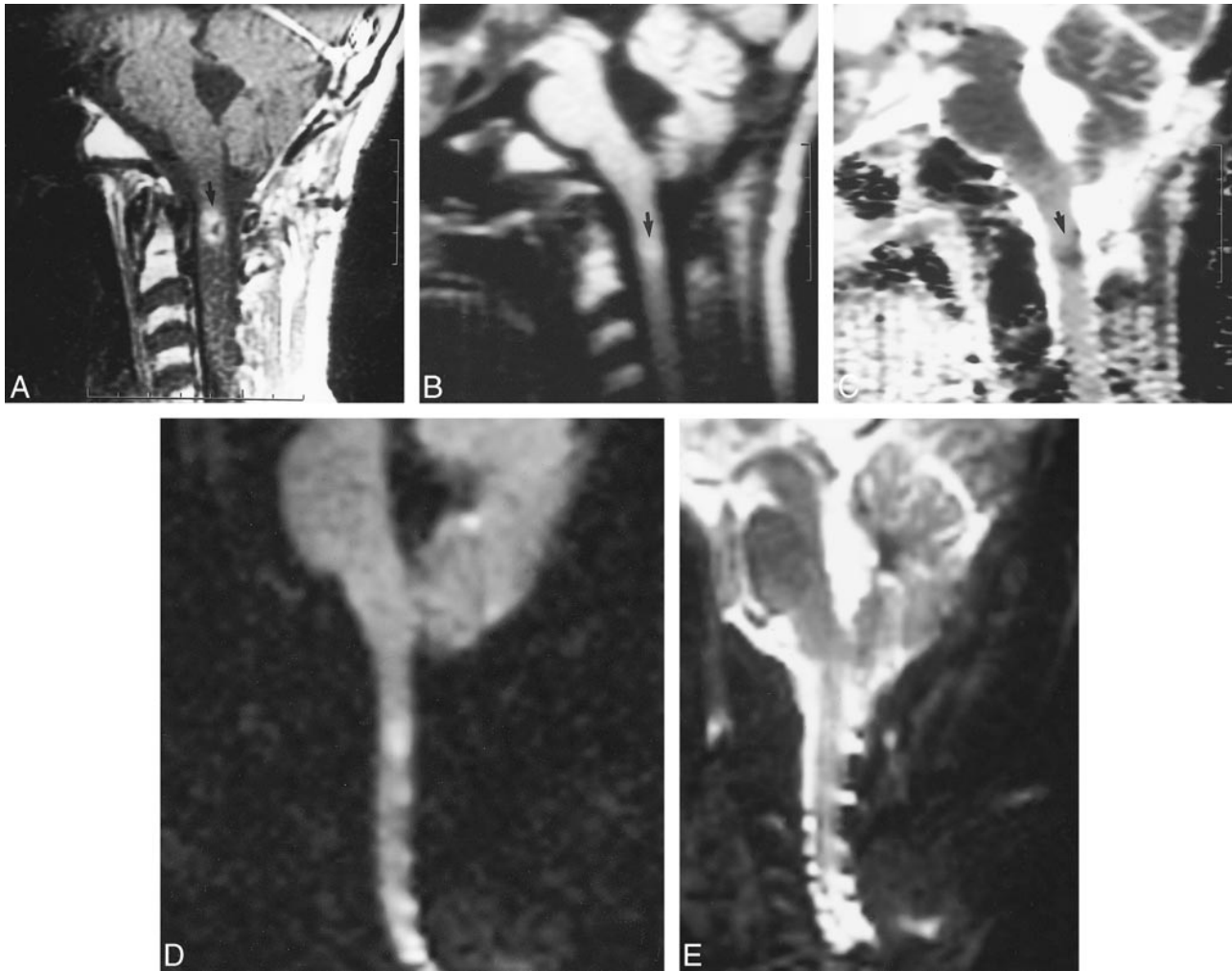


FIG 2. Case of a 16-year-old male patient with medulloblastoma treated with craniospinal radiation with presumed radiation effect at the site of overlap of the cranial and spinal radiation fields in the upper cervical spinal cord. Based on the intramedullary location of the lesion, metastatic medulloblastoma was considered unlikely. On follow-up images several months later (not shown) the lesion resolved. No anti-cancer therapy was undertaken during that time, and radiation effect was therefore considered to have been the most likely cause of the lesion.

A, Sagittal contrast-enhanced T1-weighted image (600/20/2) of the cervical spine shows intramedullary enhancement (*arrow*).

B, Sagittal LSDI isotropic high  $b$  factor diffusion image (2014/95/1, 4-mm section thickness,  $b = 750$  s/mm<sup>2</sup> extrapolated to 1000 s/mm<sup>2</sup>, six directions) shows increased signal within the lesion (*arrow*).

C, Sagittal LSDI trace ADC map shows low intensity within the lesion confirming decreased diffusion (*arrow*).

D, Sagittal EPDI isotropic high  $b$  factor diffusion image (4999/108/1, 5-mm section thickness,  $b = 1000$  s/mm<sup>2</sup>, three directions) shows artifactual high signal intensity in multiple locations in the cervical spinal cord.

E, Sagittal EPDI trace ADC map is degraded by artifact and does not show the lesion seen on both the conventional MR and the LSDI sequences.

igated spin-echo technique, pulsed-gradient spin-echo diffusion imaging (2, 8–15). Diffusion anisotropy within the spinal cord is presumed to be largely due to the directionality of the white matter fiber tracts. Based on high-field *in vitro* experiments, anisotropic diffusion has also been shown in spinal cord gray matter, although the observed anisotropy is less than that of white matter (8, 10, 11). It is important to recognize that, in this study, our reported values of RA are only qualitative because the determination of RA depends on the diffusion gradient directions sampled with respect to the axis of the spine. *In vivo*, the spinal cord is a curved structure and therefore is not consistently aligned with the gradient axes. Thus, full diffusion tensor studies

and analyses are required before quantitative statements regarding rotationally invariant anisotropic quantities can be made. This subject is beyond the scope of the present study in which the primary reason for sampling multiple diffusion gradient directions was to obtain rotationally invariant trace ADC maps. Also, because the ROI measurements made in our study included both gray matter and white matter, the obtained values reflect a combination of the RA of these tissues. The inconsistency of alignment between the spinal cord and the diffusion gradient axes combined with the partial volume averaging of gray and white matter in the ROI measurements made in this study likely contributed to the wide range of diffusion anisotropy measure-

ADC measurements ( $\mu\text{m}^2/\text{s}$ ) and RA measurements of the normal spinal cord in 10 patients

Case #	Age	Directions Measured	Location	Trace ADC	RA
1	18 y	6	T	0.96	2
2	1 y	6	T	0.91	1.41
3	16 y	6	C	0.95	1.39
4	15 y	6	C	1.06	1.48
5	11 y	3	T	0.96	1.36
6	2 y	3	C	0.91	1.58
7	3 y	3	C	0.92	1.33
8	14 y	3	C	0.91	2.3
9	2 y	3	C	0.98	2.5
10	2 mo	3	C/T/L	1.00	1.62
Mean $\pm$ SD				0.96 $\pm$ 0.05	1.70 $\pm$ 0.42

Note.—y—year; mo—month; SD—standard deviation; C—cervical spine; T—thoracic spine; L—lumbar spine.

ments obtained. The routine use of full diffusion tensor imaging and higher spatial resolution imaging would likely produce more reliable measures of diffusion anisotropy of the spinal cord.

Because LSDI can be performed more rapidly than can other currently available spin-echo techniques, such as pulsed-gradient spin-echo diffusion imaging, the diffusion characteristics of both normal and pathologic processes may be characterized using multiple diffusion gradient directions or multiple gradient  $b$  factors (4, 5). For most clinical applications, measurements of the diffusion tensor trace are likely to be more informative than the evaluation of the individual directional images or anisotropy measurements. Because the tensor trace is rotationally invariant, the calculation of the trace images does not depend on the orientation of the gradient axes with respect to the spinal cord.

The in-plane spatial resolution of 1.54 mm used in this study seemed to be diagnostically adequate for most patients; however, higher spatial resolution may be desirable in certain applications and is possible with LSDI, but at a cost of longer acquisition times. As shown in an adult volunteer, the sampling of fewer columns of data can decrease the scan time without a significant loss in the diagnostic quality of the image of the spinal cord, although less surrounding anatomy is displayed (Fig 1).

Although in the cases presented, LSDI did not alter the diagnostic considerations or therapy, the purpose of this study was to show the feasibility of the technique. Based on experience with diffusion imaging of the brain, diffusion imaging of the spinal cord will likely have important applications, especially in distinguishing acute ischemic lesions from nonischemic disorders (16, 17). The potential pediatric applications of in vivo diffusion imaging include the evaluation of normal spinal cord maturation (18) and the detection or assessment of a variety of pathologic entities such as myelin loss, ischemia, trauma, tumors, and inflammatory processes.

## References

- Chien D, Kwong K, Gress DR, Buonanno FS, Buxton RB, Rosen BR. **MR diffusion imaging of cerebral infarction in humans.** *AJNR Am J Neuroradiol* 1992;13:1097–1102
- Moseley ME, Kucharczyk J, Mintorovitch J, et al. **Diffusion MR imaging of acute stroke: correlation with T2-weighted and magnetic susceptibility-enhanced MR imaging in cats.** *AJNR Am J Neuroradiol* 1990;11:423–429
- Lovblad K, Jakob PM, Chien Q, et al. **Turbo spin-echo diffusion MR of ischemic stroke.** *AJNR Am J Neuroradiol* 1998;19:201–208
- Clark CA, Barker GJ, Tofts PS. **Magnetic resonance diffusion imaging of the human cervical spinal cord in vivo.** *Magn Res Med* 1999;41:1269–1273
- Gudbjartsson H, Maier SE, Mulkern RV, Mooczyk IA, Patz S, Jolesz FA. **Line scan diffusion imaging.** *Magn Reson Med* 1996;36:509–519
- Robertson RL, Maier SE, Robson CD, Mulkern RV, Karas PM, Barnes PD. **MR line scan diffusion imaging of the brain in children.** *AJNR Am J Neuroradiol* 1999;20:419–425
- Stejskal EO, Tanner JE. **Spin diffusion measurements: spin echoes in the presence of a time-dependent field gradient.** *J Chem Phys* 1965;42:288–292
- Ahrens ET, Laidlaw DH, Readhead C, Brosnan CF, Fraser SE, Jacobs RE. **MR microscopy of transgenic mice that spontaneously acquire experimental allergic encephalomyelitis.** *Magn Reson Med* 1998;40:119–132
- Ford JC, Hackney DB, Alsop DC, et al. **MRI characterization of diffusion coefficients in a rat spinal cord injury model.** *Magn Reson Med* 1994;31:488–494
- Gulani V, Iwamoto GA, Jiang H, Shimony JS, Webb AG, Lauterbur PC. **A multiple echo pulse sequence for diffusion tensor imaging and its application in excised rat spinal cords.** *Magn Reson Med* 1997;38:868–873
- Inglis BA, Yang L, Wirth ED III, Plant D, Mareci TH. **Diffusion anisotropy in excised normal rat spinal cord measured by NMR microscopy.** *Magn Reson Imaging* 1997;15:441–450
- Matsuzawa H, Kwee IL, Nakada T. **Magnetic resonance axonography of the rat spinal cord: postmortem effects.** *J Neurosurg* 1995;83:1023–1028
- Nakada T, Matsuzawa H, Kwee IL. **Magnetic resonance axonography of the rat spinal cord.** *Neuroreport* 1994;5:2053–2056
- Pattany PM, Puckett WR, Klose KJ, et al. **High-resolution diffusion MR of fresh and fixed cat spinal cords: evaluation of diffusion coefficients and anisotropy.** *AJNR Am J Neuroradiol* 1997;18:1049–1056
- Trudeau JD, Dixon WT, Hawkins J. **The effect of inhomogeneous sample susceptibility on measured diffusion anisotropy using NMR imaging.** *J Magn Reson B* 1995;108:22–30
- Larsson HB, Thomsen C, Frederiksen J, Stubgaard M, Henriksen O. **In vivo magnetic resonance diffusion measurement in the brain of patients with multiple sclerosis.** *Magn Reson Imaging* 1992;10:7–12
- Lutsep HL, Albers GW, DeCrespigny A, Kamat GN, Marks MP, Moseley ME. **Clinical utility of diffusion magnetic resonance**

**imaging in the assessment of ischemic stroke.** *Ann Neurol* 1997; 41:574-580

18. Zientara GP, Murphy BP, Maier SE, et al. *Diffusion Tensor MRI of the Human Cervical Spinal Cord in Vivo in Preterm Newborns*. Philadelphia: International Society of Magnetic Resonance in Medicine;1999:1099

## Appendix

For the patients in whom three directions were sampled, the diffusion gradient vector configurations sampled were (1, -1, -1/2), (1, 1/2, 1), and (1/2, 1, -1). The use of all three gradients simultaneously rather than the use of single gradient configurations along the principal axes, (1, 0, 0), (0, 1, 0), and (0, 0, 1), allows for a reduction in the echo time for a given  $b$  factor, reducing signal loss due to T2 decay and improving SNR. The effective diffusion coefficients along each of the three directions is, however, somewhat more complicated in terms of the diffusion tensor elements than single principal axis sampling. Denoting as  $D_{i,j,k}$  the diffusion coefficient measured along the direction (i,j,k), the effective diffusion coefficients along each axis read as follows.

$$D_{1,-1,-1/2} = D_{xx} + D_{yy} + D_{zz}/4 - D_{xz} + D_{yz} - 2D_{xy} \quad (1A)$$

$$D_{1,1/2,1} = D_{xx} + D_{zz} + D_{yy}/4 + D_{xy} + D_{yz} + 2D_{xz} \quad (1B)$$

$$D_{1/2,1,-1} = D_{yy} + D_{zz} + D_{xx}/4 + D_{xy} - D_{xz} - 2D_{yz} \quad (1C)$$

$D_{xx}$ ,  $D_{yy}$ , and  $D_{zz}$  are the diagonal elements of the diffusion tensor, which are equal to each other for isotropic diffusion.  $D_{xy}$ ,  $D_{xz}$ , and  $D_{yz}$  are the off-diagonal elements that vanish in the case of isotropic diffusion. Summing equations [1A] through [1C] cancels off-diagonal terms and leaves a quantity equal to nine fourths of the trace, or the sum of the diagonal

elements. ADCs are defined as one third of the trace, or the average of the diagonal elements.

For isotropic diffusion in which the diagonal elements of the diffusion tensor are equal and the off-diagonal elements vanish, ratios of any two of the diffusion coefficients defined in equations [1A] through [1C] will yield unity. The departure of such ratios from unity offers one measure of diffusion anisotropy, although others can be used. Thus, a measure of RA may be defined as the ratio of the maximum to minimum ADC obtained from the three separate ADC measurements made along the directions characterized by equations [1A] through [1C].

For the patients in whom six directions were sampled, a more complete characterization of the diffusion tensor elements and anisotropic properties is available. The six gradient configurations sampled are given by the directional vectors (1, 1, 0), (-1, 1, 0), (1, 0, 1), (-1, 0, 1), (0, 1, 1), and (0, -1, 1). The use of only two gradient axes per configuration requires lengthening the TE to accommodate the same diffusion weighting as for the diffusion sensitization configuration discussed in the previous paragraphs. Denoting as  $D_{ijk}$  the diffusion coefficient measured along the direction (i,j,k), the trace of the diffusion tensor is given by the following.

$$\begin{aligned} \text{Trace} &= D_{xx} + D_{yy} + D_{zz} \\ &= (D_{110} + D_{101} + D_{011} + D_{-110} \\ &\quad + D_{-101} + D_{0-11})/4 \end{aligned} \quad (2A)$$

The individual diagonal and off-diagonal elements may be calculated with the following relations.

$$D_{zz} = \text{Trace} - (D_{-110} + D_{110})/2 \quad (2B)$$

$$D_{yy} = \text{Trace} - (D_{101} + D_{-101})/2 \quad (2C)$$

$$D_{xx} = \text{Trace} - (D_{0-11} + D_{011})/2 \quad (2D)$$

$$D_{xy} = (D_{110} - D_{-110})/4 \quad (2E)$$

$$D_{xz} = (D_{101} - D_{-101})/4 \quad (2F)$$

$$D_{yz} = (D_{011} - D_{0-11})/4 \quad (2G)$$